Published in final edited form as:
Curr Biol. 2016 November 07; 26(21): 2942–2950. doi:10.1016/j.cub.2016.08.057.

Epithelial cell packing induces distinct modes of cell extrusions

Leyla Kocgozlu[#1], **Thuan Beng Saw**[#1,2], **Anh Phuong Le**[1,2], **Ivan Yow**[1], **Murat Shagirov**[1], **Eunice Wong**[1], **René-Marc Mège**[3], **Chwee Teck Lim**[1,4], **Yusuke Toyama**[1,5,6,**], and **Benoit Ladoux**[1,3,**]

[1]Mechanobiology Institute, National University of Singapore, T-Lab, 5A Engineering Drive 1, 117411, Singapore

[2]National University of Singapore Graduate School for Integrative Sciences and Engineering (NGS), National University of Singapore, Centre for Life Sciences (CeLS), #05-01, 28 Medical Drive, 117456, Singapore

[3]Institut Jacques Monod (IJM), CNRS UMR 7592 & Université Paris Diderot, 15 rue Hélène Brion, 75013, Paris, France

[4]Department of Biomedical Engineering, Faculty of Engineering, National University of Singapore, Block E4, #04-08, 4 Engineering Drive 3, 117583, Singapore

[5]Department of Biological Sciences, National University of Singapore, 14 Science Drive 4, 117543, Singapore

[6]Temasek Life Sciences Laboratory, 1 Research Link, National University of Singapore, 117604, Singapore

[#] These authors contributed equally to this work.

Summary

The control of tissue growth, which is a key to maintain the protective barrier function of the epithelium, depends on the balance between cell division and cell extrusion rates [1, 2]. Cells within confluent epithelial layers undergo cell extrusion, which relies on cell-cell interactions [3] and actomyosin contractility [4, 5]. Although it has been reported that cell extrusion is also dependent on cell density [6, 7], the contribution of tissue mechanics, which is tightly regulated by cell density [8–12], to cell extrusion is still poorly understood. By measuring the multi-cellular dynamics and traction forces, we show that changes in epithelial packing density lead to the emergence of distinct modes of cell extrusion. In confluent epithelia with low cell density, cell extrusion is mainly driven by the lamellipodia-based crawling mechanism in the neighbor non-dying cells in connection with large-scale collective movements. As cell density increases, cell motion is shown to slow down and the role of a supra-cellular actomyosin cable formation and its contraction in the neighboring cells becomes the preponderant mechanism to locally promote cell

[**]Corresponding authors, Lead contact : Benoit Ladoux, benoit.ladoux@ijm.fr; Additional corresponding author: Yusuke Toyama, dbsty@nus.edu.sg.

Author Contributions

Y.T and B.L. designed research, L.K., T.B.S., A.P.L., I.Y., E.W., Y.T. performed experiments, L.K., T.B.S, M.S., C.T.L., R.M.M., Y.T., B.L. contributed new reagents and computational tools, L.K., T.B.S., M.S., Y.T., B.L. analyzed the data, L.K., T.B.S., Y.T., B.L. wrote the paper, Y.T. and B.L. supervised the project. All authors read the manuscript and commented on it.

Europe PMC Funders Author Manuscripts

Europe PMC Funders Author Manuscripts

extrusion. We propose that these two distinct mechanisms complement each other to ensure proper cell extrusion depending on the cellular environment. Our study provides a quantitative and robust framework to explain how cell density can influence tissue mechanics and in turn, regulate cell extrusion mechanism.

Results and Discussion

Preserving the integrity of epithelial barriers during cell extrusion requires rearrangements of neighboring cells around the extruding cell [3]. The progression of cell extrusion in epithelial sheets, particularly apoptotic cell extrusion, has been largely associated with local movements of neighboring cells driven by the formation and contraction of actomyosin rings [3–5, 13, 14], so called purse-string mechanism. However, the interdependence of cell extrusion events and the overall remodeling of tissues has not been explored to date. The sealing of epithelial gaps observed during wound healing or morphogenetic events [15–18] largely depends on mechanical factors [14, 19, 20]. Such factors would promote either the assembly of actomyosin cables or cell crawling to efficiently seal epithelial gaps [14, 19]. In addition, as cell density increases within epithelial tissues, large scale coordinated movements are reduced to local dynamics, impacting cell-substrate and cell-cell interactions [8, 10]. Even though the impact of mechanics has been evidenced for gap closure during wound healing or morphogenesis, the contributions of tissue mechanics and dynamics remain to be determined in the context of epithelial gap sealing during cell extrusion.

To control the growth and the cell density of epithelial monolayers, we used micro-patterned adherent substrates [21–23]. We first followed cell extrusion over time as a function of cell density by culturing Madin-Darby canine kidney (MDCK) cells on circular patterns with typical radius, r of 250 μm (Figure 1A, Movie S1-left). The average number of cells increased over time, with a higher growth rate at low cell density, i.e. ~$0.8 \cdot (100\ \mu m)^{-2} \cdot hr^{-1}$ at a density of ≤33 cells per $(100\ \mu m)^2$ (phase 1) than at higher cell density, i.e. ~$0.5 \cdot (100\ \mu m)^{-2} \cdot hr^{-1}$ at a density of ≥37 cells per $(100\ \mu m)^2$ (phase 2), suggesting two different phases in tissue growth (Figure 1B). Even though cells remain adherent to the substrate under these different culture conditions, cell-substrate adhesion is also affected between these two phases as shown by the size of focal adhesions (Figure 1C). We found that most of the cell extrusions in both phases were associated with the characteristics of apoptosis (caspase-3 activation, and nuclear condensation and/or fragmentation), indicating that these events were apoptotic cell extrusions (Figure 1D, Movie S2). The cumulative number of cell extrusion events increased with time (Figure 1E), and the rate of cell extrusion increased five-fold between phase 1 and 2 (Figure 1F). The minor spatial bias in cell density (a slightly higher density at the tissue edge in phase 1) did not incur any significant non-uniformity in the spatial distribution of cell division and extrusion (Figures S1A-C), allowing us to analyze the monolayer as a whole. Moreover, we verified that the rate of cell extrusions did not alter with high cell seeding densities, i.e. similar to phase 2, or without spatial constraint, i.e. similar to a non-constraint tissue expanding into the void (Figure S1D).

To investigate the relationship between cell extrusion and tissue dynamics, we analyzed the velocity field by using Particle Image Velocimetry (PIV) [24, 25] (movie S1-right). The

average speed over the entire tissue showed two distinct regimes (Figure 1G): a slow decrease during the first ~10 hours (phase 1) followed by a large reduction of the speed during phase 2. This was consistent with previous findings that tightly packed tissue could lead to a globally breathless state [26]. The global fluctuations of cell velocities, which were previously described [10], also showed changes with respect to density (Figure 1H). In particular, we observed the emergence of radial oscillations as shown by alternate bands of positive and negative values of average radial velocity that gradually decreased as cell density rises. The large-scale displacements (with average velocity -8 μm/hr to +8 μm/hr) that spanned over the whole tissue during phase 1 changed signs every few hours. These oscillations gradually subsided in magnitude as density increased, which corresponded to phase 2 (Figure 1H). These results may explain the observed differences in cell extrusion as cell density increases. At low global cell density, large-scale movements of the tissue could lead to transient increases in density in certain parts of the tissue that favor cell extrusion in those areas, whereas at high global density, the environment is packed everywhere in the tissue and extrusions can thus occur at any location and time, increasing significantly the total extrusion rate in phase 2 compared to phase 1 (Figure 1F). In particular, during phase 1, extrusions mainly occurred when the global average radial velocity was pointing towards the center (positive global $<V_r>$) of the tissue (Figure S1E), which resulted in the total extrusion rate becoming significantly lower when the tissue globally moved away from the tissue center (Figure S1F).

In addition to tissue dynamics, we measured the evolution of the global traction forces exerted by MDCK cells over time using micropillar substrates [27, 28]. The analysis of the overall forces showed that both the average traction force magnitude, $<|T(\rho)|>$ (Figure 1I), and the average traction force magnitude restricted to the edge of the circular patterns, $<|T(\rho)|_{edge}>$ (Figure 1J), where the largest forces were usually observed [27, 29], decreased with the increase of cell density. The average traction force, $<T(\rho)>$ changed direction, from forces pointing globally inwards to the tissue (positive) to outward (negative) at higher densities, suggesting that the tissue changed from a global contractile state to a more compressive state reaching higher internal pressure (Figure 1K). Altogether, these results show that the differences observed in the number and rate of extrusions between phase 1 and 2 are correlated with global changes in the physical properties of epithelial cells.

We next investigated the epithelial tissue remodeling induced by cell extrusion in the two phases. Previous studies have shown that cell extrusion was associated with the deformation of surrounding neighbor cells [4]. We thus analyzed the dynamics of cells around the extrusion site using PIV measurements as a function of the distance from the extruding cell up to a radius of ~150 μm. Typical examples of color-coded velocity map of the radial component of PIV around extrusion sites (Figure 2A) for phases 1 and 2 are shown in Figures 2B-C, respectively (t=0 min denotes the initiation of extrusion, Supplemental Experimental Procedures). At lower density (phase 1), there was a gradual buildup of net movement of surrounding cells towards the extrusion site before the extrusion (t=-50 min in Figure 2B). Right after the extrusion (t=+10 min), the net velocity towards the extrusion became more prominent, radially uniform, and extended up to many cell rows away from the extrusion site. As time progressed, cells started to lose their movement in the direction of extrusion, starting from the innermost cells (t=+90 min), and progressing to the outer cells

(t=+150 min). At higher density (phase 2), we also observed a local directed motion associated with extrusion but over a shorter distance and time, and with smaller velocity magnitude in comparison to phase 1 (Figure 2C).

To quantify the tissue dynamics associated with the extrusion, we plotted the kymograph of average radial velocity, $<V_r>$ as a function of distance from the extrusion site (Figures 2D-E), and statistically compared them to similar plots for areas not associated with cell extrusion (Figures S1G-J, Supplemental Experimental Procedures). The dynamics associated with the extrusion and statistically distinguished from background dynamics (the region delineated in Figure 2E) show that the neighboring tissue moved toward the extrusion, with distinct characteristic propagation lengths, l_v in phase 1 and 2 (Figures 2E-F, Supplemental Experimental Procedures). In phase 1 upon extrusion (t=0 min), l_v shows that cells within a ~125 μm radius around the extrusion (~6 cells) exhibited a high and positive radial velocity (red-orange-yellow region, Figure 2E), starting from the cells closest to the extrusion. The progressive mobilization of more distant cells (denoted by the slant of the delineated region in Figure 2E) is reminiscent of collective cell movements reported for epithelial monolayer expansion into multicellular-sized voids, and attributed to mechanical sensing and propagation of mechanical information [30]. We further analyzed the local cell density around the extrusion (within a radius of 20-30 μm) and found that the cell density started to increase before the cell extrusion (Figure 2G). We speculate that the transient flow toward the extrusion site prior to the extrusion (arrow in Figure 2E) led to a transient and local density increase, which could favor cell extrusion. Similarly, in phase 2, we observed an increase in the average positive radial velocity, which correlated with the extrusion time (Figure 2D), but the cells with high positive velocity were significantly reduced and more spatially restricted to the vicinity of the extrusion site (delineated region in Figure 2E, l_v ~60 μm, Figure 2F) and less cells were involved (~4 cells) compared to phase 1. This is in line with our observations that cells further away from the extrusion moved less towards the extrusion (Figure 2C). The duration of inward movements was shorter in phase 2 (<1 hr) than in phase 1. At high density, extrusions were not linked to significant local density changes (Figure 2G). Altogether, these analyses show that distinct multicellular dynamics with respect to global cell density are at play during cell extrusion. At low density, the extrusion process is associated with long-range tissue flow that modifies the local cell density and favors cell extrusion. At high density, cell movements are restricted to the cell extrusion site.

As cell migration and actomyosin contraction have been shown to mutually interact in other epithelial gap closure mechanisms than extrusion such as wound healing [17–19], we then investigate the roles of cell crawling [14, 31], actomyosin contractility [4, 5, 13] and cell-cell junctions [3, 32] in the context of cell extrusion. To this end, we used α-catenin knock-down (KD) cells [33–35] that are unable to form proper cell-cell junctions, as well as wild-type cells treated with blebbistatin (50 μM) and NSC23766 (200 μM) in order to inhibit Myosin II and Rac1, respectively. We first measured the propagation length, l_v (Figure 3A) from the kymographs of average radial velocity, $<V_r>$ for each condition (Figures S2A-B). In phase 2, only blebbistatin treatment significantly reduced l_v compared to control condition, suggesting a mechanism largely driven by actomyosin based contractility as previously described [3–5, 13]. In contrast, in phase 1, l_v was significantly reduced in all conditions to

roughly half of its length as compared to control case (Figure 3A). Notably, the inhibition of Rac1 significantly reduced l_v in phase 1 but not in phase 2 compared to each controls. This suggests that the mechanisms giving rise to the long-range extrusion-directed motion in phase 1 (and not phase 2) is Rac1-based cell migration, while the shorter-range tissue movement in phase 2 is mostly driven by actomyosin contraction.

To further clarify the contribution of lamellipodia-based crawling mechanism and purse-string contractile mechanism during cell extrusion, we used UV laser to induce apoptotic extrusion [5, 36] (Supplemental Experimental Procedures), and followed the evolution of the extrusion at high spatio-temporal resolution using confocal microscopy. We co-cultured MDCK cells that expressed GFP-labelled F-actin (or myosin light chain) and non-labeled control cells, and induced apoptosis to a non-GFP cell surrounded by GFP positive cells (Figures 3B, S3A and S3B) to unambiguously follow how the extruding cell changes its area over time. We compared these control results with (S)-nitro-blebbistatin (SBB)- and NSC23766-treated cells. The effect of the drug treatments to the cell extrusion was measured by tracking the apical area of extruding cell over time (Figures S3C-D), and quantified with Kaplan-Meier survival plots (Figure 3C, Supplemental Experimental Procedures). In phase 1, only NSC23766 treatment significantly delayed the area shrinkage with respect to non-drugged condition (Figure 3C). NSC23766-treated cells typically did not complete even after 300 - 600 min, while the extrusion process of control cells usually completed within 100 - 150 min (Figure S3C). In contrast, in phase 2, the extrusion process largely slowed down under SBB treatment (Figure 3C). This analysis thus strengthened the idea that lamellipodia-based crawling mechanism is the main driving force of gap closure during extrusion in phase 1, and this process switches to a more purse-string-based contractile mechanism at higher density.

To test this hypothesis, we examined the cytoskeletal and molecular changes in the immediate neighbors of an extruding cell. To this end, we monitored GFP-tagged F-actin (actin-GFP), YFP-tagged p21-binding domain (PBD–YFP) probe of activated Rac1 and Cdc42 [37], and GFP-tagged myosin light chain (myosin-GFP) in the neighboring cells. At low density (phase 1), upon caspase-3 activation (t=0 min in Figures 4A-C), the nearest-neighbor cells formed lamellipodia, and extended these protrusions into the area originally occupied by the apoptotic cell within ~1.5 hrs (arrowheads in Figures 4B-C, Movie S3-top). This lamellipodia extension was associated with the detachment of apoptotic cell from the substrate, characterized by the retraction of stress fibers in the apoptotic cell (Figure S4c and Movie S5). This observation was consistent with a previous report showing that caspase-3 can compromise cell adhesion by cleaving adhesion components [38], and strongly suggested that lamellipodia-based crawling helps to directly push the apoptotic cell out of the monolayer. In addition, we observed that actin accumulation at the apical side of the cell started only after the lamellipodia filled the space below the dying cell (arrows in Figures 4A and 4C, apical), suggesting a secondary role for the purse-string mechanism. At high cell density (phase 2), as previously described [3–5, 13], there was accumulation of actin at the apical side of the neighboring cell (arrow in Figure 4D, t=15 min) that later moved toward the basal side of the cell (arrow in Figure 4E, t=25 min) upon caspase-3 activation (Figure 4F, Movie S4) suggesting a mechanism driven by purse-string. Moreover, little or no lamellipodia were observed in phase 2.

These two distinct mechanisms were further confirmed by monitoring PBD-YFP and myosin-GFP. In particular, the PBD-YFP signal at the basal section of neighbor-extruding cell interface was clearly activated upon the initiation of extrusion (Figure 4G, t=0 min) in phase 1, but not in phase 2 (arrows in Figure 4G and arrowheads in Figure 4H), suggesting a lamellipodia-based mechanism in phase 1. In contrast, there was accumulation of myosin-GFP along the neighbor-extruding cell interface in phase 2 (arrows in Figure S3F), but myosin-GFP accumulated only at a small segment of the neighbor-extruding cell interface throughout most of the extrusion process in phase 1 (arrows in Figure S3G).

Lamellipodia-based protrusions and purse-string mechanism have been reported to lead to different signatures of traction force distribution [19, 39]. We thus measured the traction forces exerted by epithelial cells during cell extrusion, and computed radial traction forces as a function of distance around the extrusion site (Figure 4I, Supplemental Experimental Procedures). At low density (phase 1), we first observed traction forces underneath the apoptotic cell predominantly pointed radially toward the extruding cell, likely corresponding to the forces exerted by the contraction of stress fibers (Figure S3E, Movie S3-bottom) within 20 μm and ~1 hr before the extrusion (green vectors in Figure 4J, t=-50 min). Upon extrusion, these traction forces decreased, probably due to de-adhesion of the apoptotic cell through caspase activation (Figure S3E, Movie S3-bottom). Shortly after the onset of extrusion, the traction forces predominantly pointed radially away from the extruding cell (red vectors in Figure 4J, t=30 min) at the interface between extruding and neighboring cells, which is in good agreement with a lamellipodia-based mechanism as previously observed [39]. The average radial traction force kymograph quantifying the spatio-temporal patterns of the traction forces around extrusions (Figure 4L) was statistically compared with that of areas not associated with cell extrusion (Figure S3H), and further supported our observations (Figure 4J). The traction forces associated with cell extrusion (colored regions in Figure 4L, Supplemental Experimental Procedures) at the vicinity of extruding cell ($r < 10$ μm) showed strong negative values after extrusion (arrow in Figure 4L), and gradually decreased thereafter. In addition, regular patches of negative (i.e. away from the extrusion and into the tissue) forces propagated over time to reach larger radii (arrowheads in Figure 4L). This is in agreement with collective and progressive mobilization of multiple cells towards the extrusion site (Figures 2B and 2E) through a lamellipodia-based mechanism. At high density (phase 2), the magnitude of traction forces was largely reduced and there were no clearly discernible traction patterns (colored regions in Figure 4M). Notably, the average radial traction force kymograph did not show negative forces after extrusion at the vicinity of extruding cell ($r<10$ μm), in contrast to the post-extrusion patterns in phase 1 (Figure 4L). Moreover, there was only a weak and transient negative force patch after extrusion ($r\geq20$ μm) that did not propagate, consistent with the vectors observed in Figure 4K (t=20 min). These data showed that the signature of traction forces associated with the cell extrusion strongly depends on the cell packing density. As cell density increases, there is a corresponding decrease in overall dynamics and coordinated movements over multiple cells towards the extrusion site, which correlates with two distinct modes of cell extrusion we found in this study.

Conclusions

We showed that tissue dynamics that depend on cell packing density lead either to large-scale coordinated movements through cell crawling at low density, or to a local actomyosin contractile process of immediate neighbors to drive extrusion at high density to extrude apoptotic cells (Figure 4N). The mechanisms by which cells are extruded from epithelial sheets reported in this study are qualitatively distinct from any previous observations [3–7, 13]. Our study reveals that the emergence of various modes of cell extrusion is governed by mechanical environmental factors, which could be important for ensuring the removal of unnecessary cells (e.g., apoptotic cells) in different circumstances. Our findings provide a quantitative and robust framework to explain how internal mechanics within epithelial tissues regulates cell extrusion mechanisms.

Supplemental Information

Refer to Web version on PubMed Central for supplementary material.

Acknowledgments

The authors thank Tianchi Chen, Alexandre Kabla, Man Chun Leong, Emmanuelle N'Guyen, Julia Peukes, Andrea Ravasio, group members from MBI and Institut Jacques Monod. The authors would also like to thank MBI Microfabrication core (Gianluca Grenci and Mohammed Ashraf), MBI Science Communication core (Andrew Wong and Steven Wolf) and MBI Microscopy core (Felix Margadant) for continuous support. The authors are grateful to S. Yonemura, W. J. Nelson and Fernando Martin-Belmonte for their generous gift of MDCK cell lines. Financial supports from the Human Frontier Science Program (grant RGP0040/2012 to C.T.L., R.M.M., B.L.), the European Research Council under the European Union's Seventh Framework Programme (FP7/2007-2013 to B.L) / ERC grant agreement n° 617233 (to B.L.), Agence Nationale pour la Recherche project "PillarCell" (ANR 13-NANO-0011 to B.L.), the LABEX "Who am I?", University of Singapore Startup Grants (to Y.T.), and a Singapore Ministry of Education Tier 2 grant (MOE2015-T2-1-116 to Y.T.) and the Mechanobiology Institute (to C.T.L., Y.T., B.L.) are gratefully acknowledged. T.B.S. and A.P.L. are supported by an NGS scholarship.

References

1. Reinsch S, Karsenti E. Orientation of spindle axis and distribution of plasma membrane proteins during cell division in polarized MDCKII cells. The Journal of cell biology. 1994; 126:1509–1526. [PubMed: 8089182]
2. Farhadifar R, Roper JC, Aigouy B, Eaton S, Julicher F. The influence of cell mechanics, cell-cell interactions, and proliferation on epithelial packing. Current biology : CB. 2007; 17:2095–2104. [PubMed: 18082406]
3. Lubkov V, Bar-Sagi D. E-cadherin-mediated cell coupling is required for apoptotic cell extrusion. Current Biology. 2014; 24:868–874. [PubMed: 24704076]
4. Rosenblatt J, Raff MC, Cramer LP. An epithelial cell destined for apoptosis signals its neighbors to extrude it by an actin-and myosin-dependent mechanism. Current biology. 2001; 11:1847–1857. [PubMed: 11728307]
5. Kuipers D, Mehonic A, Kajita M, Peter L, Fujita Y, Duke T, Charras G, Gale JE. Epithelial repair is a two-stage process driven first by dying cells and then by their neighbours. Journal of cell science. 2014; 127:1229–1241. [PubMed: 24463819]
6. Marinari E, Mehonic A, Curran S, Gale J, Duke T, Baum B. Live-cell delamination counterbalances epithelial growth to limit tissue overcrowding. Nature. 2012; 484:542–545. [PubMed: 22504180]
7. Eisenhoffer GT, Loftus PD, Yoshigi M, Otsuna H, Chien C-B, Morcos PA, Rosenblatt J. Crowding induces live cell extrusion to maintain homeostatic cell numbers in epithelia. Nature. 2012; 484:546–549. [PubMed: 22504183]

Europe PMC Funders Author Manuscripts

8. Angelini TE, Hannezo E, Trepat X, Marquez M, Fredberg JJ, Weitz DA. Glass-like dynamics of collective cell migration. Proceedings of the National Academy of Sciences of the United States of America. 2011; 108:4714–4719. [PubMed: 21321233]
9. Vedula SRK, Leong MC, Lai TL, Hersen P, Kabla AJ, Lim CT, Ladoux B. Emerging modes of collective cell migration induced by geometrical constraints. Proceedings of the National Academy of Sciences of the United States of America. 2012; 109:12974–12979. [PubMed: 22814373]
10. Deforet M, Hakim V, Yevick H, Duclos G, Silberzan P. Emergence of collective modes and tri-dimensional structures from epithelial confinement. Nature communications. 2014; 5
11. Tambe DT, Hardin CC, Angelini TE, Rajendran K, Park CY, Serra-Picamal X, Zhou EHH, Zaman MH, Butler JP, Weitz DA, et al. Collective cell guidance by cooperative intercellular forces. Nature Materials. 2011; 10:469–475. [PubMed: 21602808]
12. Vedula SRK, Hirata H, Nai MH, Toyama Y, Trepat X, Lim CT, Ladoux B. Epithelial bridges maintain tissue integrity during collective cell migration. Nature materials. 2014; 13:87–96. [PubMed: 24292420]
13. Wu SK, Gomez GA, Michael M, Verma S, Cox HL, Lefevre JG, Parton RG, Hamilton NA, Neufeld Z, Yap AS. Cortical F-actin stabilization generates apical–lateral patterns of junctional contractility that integrate cells into epithelia. Nature cell biology. 2014; 16:167–178. [PubMed: 24413434]
14. Anon E, Serra-Picamal X, Hersen P, Gauthier NC, Sheetz MP, Trepat X, Ladoux B. Cell crawling mediates collective cell migration to close undamaged epithelial gaps. Proceedings of the National Academy of Sciences. 2012; 109:10891–10896.
15. Tamada M, Perez TD, Nelson WJ, Sheetz MP. Two distinct modes of myosin assembly and dynamics during epithelial wound closure. Journal of Cell Biology. 2007; 176:27–33. [PubMed: 17200415]
16. Matsubayashi Y, Razzell W, Martin P. 'White wave'analysis of epithelial scratch wound healing reveals how cells mobilise back from the leading edge in a myosin-II-dependent fashion. Journal of cell science. 2011; 124:1017–1021. [PubMed: 21402875]
17. Wood W, Jacinto A, Grose R, Woolner S, Gale J, Wilson C, Martin P. Wound healing recapitulates morphogenesis in Drosophila embryos. Nature cell biology. 2002; 4:907–912. [PubMed: 12402048]
18. Klarlund JK. Dual modes of motility at the leading edge of migrating epithelial cell sheets. Proceedings of the National Academy of Sciences. 2012; 109:15799–15804.
19. Ravasio A, Cheddadi I, Chen T, Pereira T, Ong HT, Bertocchi C, Brugues A, Jacinto A, Kabla AJ, Toyama Y, et al. Gap geometry dictates epithelial closure efficiency. Nature communications. 2015; 6
20. Reffay M, Parrini M-C, Cochet-Escartin O, Ladoux B, Buguin A, Coscoy S, Amblard F, Camonis J, Silberzan P. Interplay of RhoA and mechanical forces in collective cell migration driven by leader cells. Nature cell biology. 2014; 16:217–223. [PubMed: 24561621]
21. Thery M. Micropatterning as a tool to decipher cell morphogenesis and functions. Journal of Cell Science. 2010; 123:4201–4213. [PubMed: 21123618]
22. Nelson CM, Jean RP, Tan JL, Liu WF, Sniadecki NJ, Spector AA, Chen CS. Emergent patterns of growth controlled by multicellular form and mechanics. Proceedings of the National Academy of Sciences of the United States of America. 2005; 102:11594–11599. [PubMed: 16049098]
23. Rolli CG, Nakayama H, Yamaguchi K, Spatz JP, Kemkemer R, Nakanishi J. Switchable adhesive substrates: revealing geometry dependence in collective cell behavior. Biomaterials. 2012; 33:2409–2418. [PubMed: 22197568]
24. Thielicke W, Stamhuis EJ. PIVlab–Towards user-friendly, affordable and accurate digital particle image velocimetry in MATLAB. Journal of Open Research Software. 2014; 2:e30.
25. Petitjean L, Reffay M, Grasland-Mongrain E, Poujade M, Ladoux B, Buguin A, Silberzan P. Velocity fields in a collectively migrating epithelium. Biophysical journal. 2010; 98:1790–1800. [PubMed: 20441742]
26. Park J-A, Kim JH, Bi D, Mitchel JA, Qazvini NT, Tantisira K, Park CY, McGill M, Kim S-H, Gweon B. Unjamming and cell shape in the asthmatic airway epithelium. Nature materials. 2015; 14:1040–1048. [PubMed: 26237129]

27. Du Roure O, Saez A, Buguin A, Austin RH, Chavrier P, Siberzan P, Ladoux B. Force mapping in epithelial cell migration. Proceedings of the National Academy of Sciences of the United States of America. 2005; 102:2390–2395. [PubMed: 15695588]
28. Gupta M, Kocgozlu L, Sarangi BR, Margadant F, Ashraf M, Ladoux B. Micropillar substrates: A tool for studying cell mechanobiology. Methods in cell biology. 2015; 125:289–308. [PubMed: 25640435]
29. Trepat X, Wasserman MR, Angelini TE, Millet E, Weitz DA, Butler JP, Fredberg JJ. Physical forces during collective cell migration. Nature physics. 2009; 5:426–430.
30. Serra-Picamal X, Conte V, Vincent R, Anon E, Tambe DT, Bazellieres E, Butler JP, Fredberg JJ, Trepat X. Mechanical waves during tissue expansion. Nature Physics. 2012; 8:628–634.
31. Poujade M, Grasland-Mongrain E, Hertzog A, Jouanneau J, Chavrier P, Ladoux B, Buguin A, Silberzan P. Collective migration of an epithelial monolayer in response to a model wound. Proceedings of the National Academy of Sciences. 2007; 104:15988–15993.
32. Grieve AG, Rabouille C. Extracellular cleavage of E-cadherin promotes epithelial cell extrusion. Journal of cell science. 2014; 127:3331–3346. [PubMed: 24895403]
33. Thomas WA, Boscher C, Chu Y-S, Cuvelier D, Martinez-Rico C, Seddiki R, Heysch J, Ladoux B, Thiery JP, Mege R-M. α-Catenin and vinculin cooperate to promote high E-cadherin-based adhesion strength. Journal of Biological Chemistry. 2013; 288:4957–4969. [PubMed: 23266828]
34. Benjamin JM, Kwiatkowski AV, Yang C, Korobova F, Pokutta S, Svitkina T, Weis WI, Nelson WJ. αE-catenin regulates actin dynamics independently of cadherin-mediated cell–cell adhesion. The Journal of cell biology. 2010; 189:339–352. [PubMed: 20404114]
35. Yonemura S, Wada Y, Watanabe T, Nagafuchi A, Shibata M. α-Catenin as a tension transducer that induces adherens junction development. Nature cell biology. 2010; 12:533–542. [PubMed: 20453849]
36. Toyama Y, Peralta XG, Wells AR, Kiehart DP, Edwards GS. Apoptotic force and tissue dynamics during Drosophila embryogenesis. Science. 2008; 321:1683–1686. [PubMed: 18802000]
37. Bryant DM, Datta A, Rodríguez-Fraticelli AE, Peränen J, Martín-Belmonte F, Mostov KE. A molecular network for de novo generation of the apical surface and lumen. Nature cell biology. 2010; 12:1035–1045. [PubMed: 20890297]
38. Levkau B, Herren B, Koyama H, Ross R, Raines EW. Caspase-mediated cleavage of focal adhesion kinase pp125FAK and disassembly of focal adhesions in human endothelial cell apoptosis. The Journal of experimental medicine. 1998; 187:579–586. [PubMed: 9463408]
39. Brugues A, Anon E, Conte V, Veldhuis JH, Gupta M, Colombelli J, Munoz JJ, Brodland GW, Ladoux B, Trepat X. Forces driving epithelial wound healing. Nature Physics. 2014; 10:684–691.

Europe PMC Funders Author Manuscripts

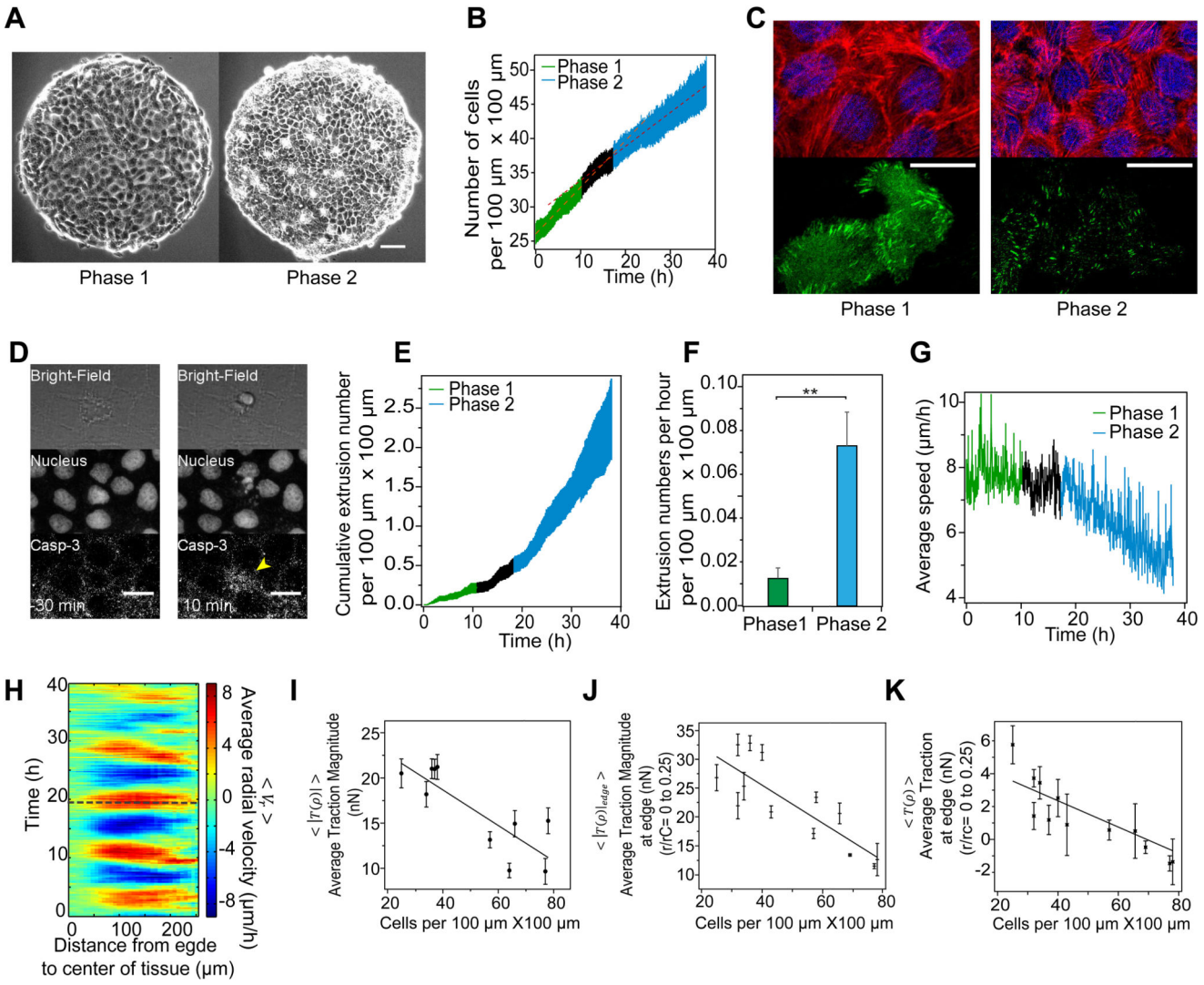

Figure 1. Dynamics and mechanical state of epithelia depend on cell packing density

(A) Phase contrast image of confined tissue on circular pattern, at low density (phase 1) and high density (phase 2), scale bar = 100 µm. (B) Average global cell density as function of time. (C) Talin-GFP (green) transfected cells at phase 1 and 2, with TRITC-phalloidin staining of F-actin (red), Hoeschst staining of nucleus (blue), scale bar = 20 µm. (D) Characteristics of apoptotic extrusion, before and after the extrusion (t= 0 min): cell rounding (bright-field image), caspase-3 positive staining (arrowhead), and nuclear fragmentation (Hoechst staining), scale bar = 20 µm. (E) Average cumulative extrusion numbers as function of time. (F) Average extrusion rate (extrusion numbers per hour), for phase 1 and 2, t-test **: p< 0.01. (G) Global average speed of tissue as function of time. (H) Kymograph of average radial velocity, $<V_r>$ from the center to the edge of tissue. The dotted line separates phase 1 (below) and phase 2 by density. (I-K) Average traction magnitude, $<|T(\rho)|>$ (I), average traction magnitude at edge of tissue, $<|T(\rho)|_{edge}>$ (J), average traction, $<T(\rho)>$ at edge of tissue (K), as a function of cell density. Values were averaged over 8

different samples for (B, D, E, F). All error bars represent standard error of mean (s.e.m.). See also Figures S1A-F.

Europe PMC Funders Author Manuscripts

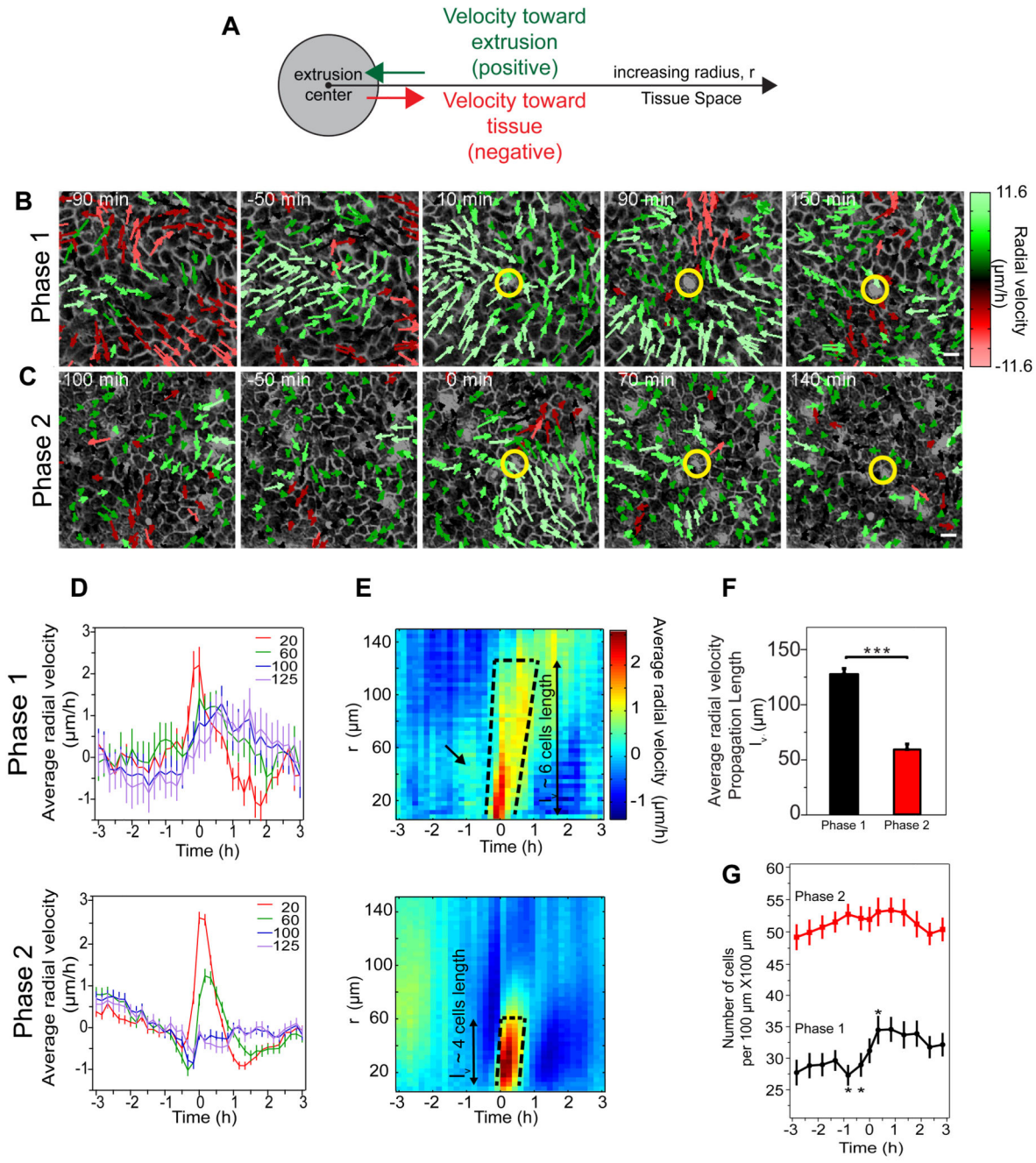

Figure 2. Distinct tissue kinematics around cell extrusion with respect to cell packing density

(A) Schematic illustrating sign convention for tissue radial velocity with respect to the center of extrusion. (B, C) Time evolution of phase contrast images of the cell extrusion event for phase 1 and 2, with velocity field vectors overlaid. Extrusion (yellow circle) occurs at t= 0 hr, in the center of the image. Length of vector is proportional to velocity magnitude, color code shows value of radial component with respect to extrusion as the center of radius. (D) Radial velocity as function of time around extrusion (t= 0 hr) averaged over all points at radius, r= 20, 60, 100, 125 μm respectively from extrusion, and averaged over all extrusion

Europe PMC Funders Author Manuscripts

events. (E) Kymograph for radial velocity data in (D). Bounded area shows approximate region with values significantly different from control (no extrusion) kymographs in Figure S1I and S1J, see Supplemental Experimental Procedures. The typical number of cells spanning the boxed area is calculated based on the typical length of the cells in each phase i.e. $l_{cell} \sim 2/\sqrt{(\pi \rho)}$, where ρ is the mean cell density in each phase. (F) The propagation length of the average radial velocity, l_v i.e. length of bounded area in (E), t-test ***: $p < 0.001$. (G) Time evolution of local cell density within radius, $r \leq 20$ μm of extrusion, averaged over all extrusions. Paired t-test comparison for extrusion event and time points within one hour around it, t-test *: $p < 0.05$. Phase 1: 8 samples, 39 events, Phase 2: 8 samples, 269 events. All error bars represent s.e.m. See also Figures S1G-J.

Europe PMC Funders Author Manuscripts

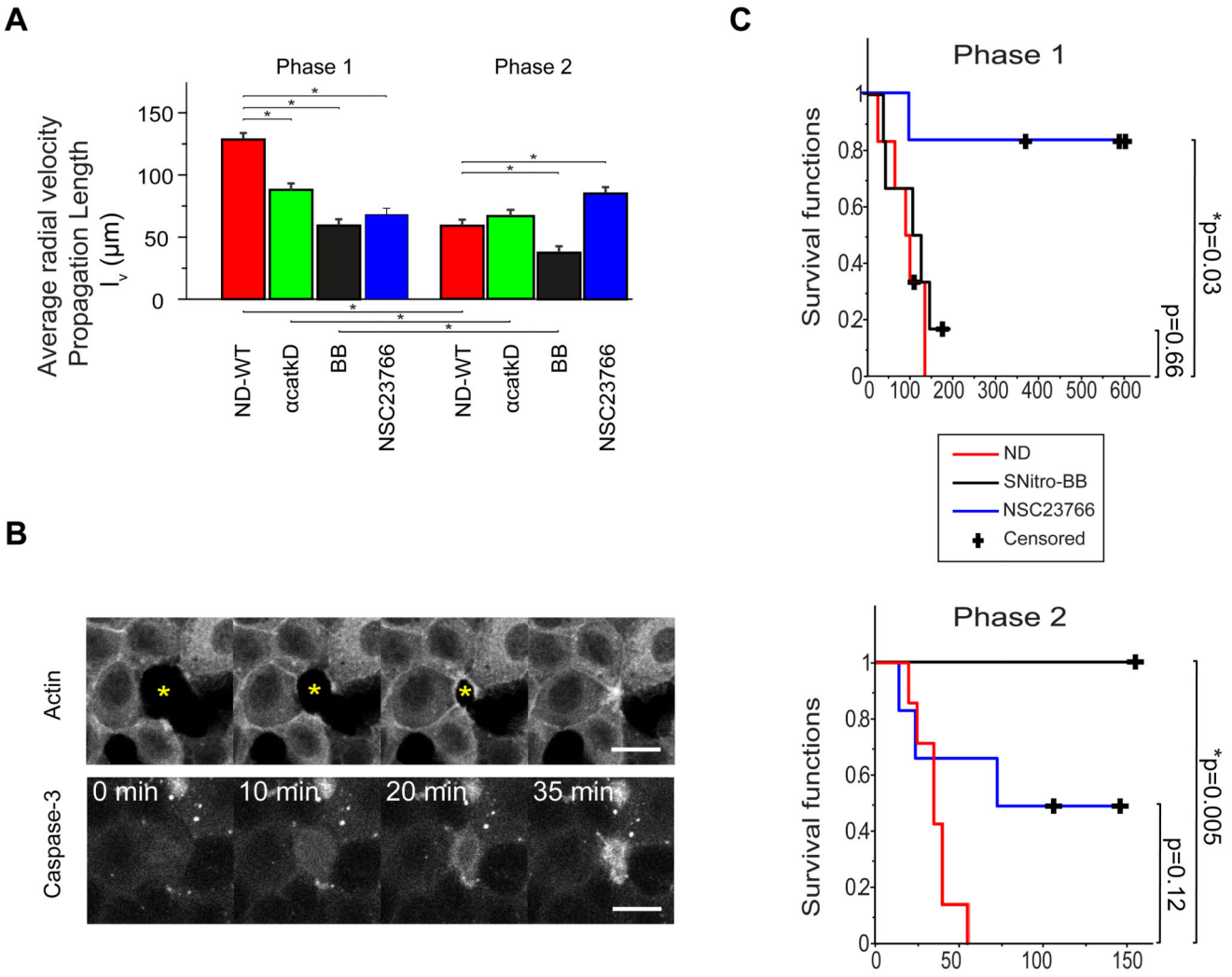

Figure 3. Distinct extrusion mechanisms in different cell packing density

(A) Comparison of propagation length of the average radial velocity, l_v measured from the corresponding kymographs in Figure S2a and S2b, for untreated WT cells (ND-WT), α-Catenin KD (αcatKD) cells, and WT cells treated with 50 μM blebbistatin (BB), or 200 μM NSC23766, during phase 1 and 2. All error bars represent s.e.m. A one-way-ANOVA was used to compare all conditions and phases, with $p \leq 10^{-21}$. Then a least significant difference post-hoc test was performed, at p= 0.01. (B) Top panel: Confocal images of a confluent monolayer with mixture of WT and actin-GFP cells with the central WT cell laser-induced for apoptotic extrusion. Extrusion at t= 0 min with the gradual shrinkage of the extruding cell (yellow asterisk) area with time. Bottom panel: Caspase-3 activation, scale bar = 20 μm. (C) Kaplan-Meier survival plots of the extruding cell area for untreated (ND - 6 extrusions each in phase 1 and 2), blebbistatin (SNitro-BB - 6 extrusions in phase 1, 5 extrusions in phase 2) and NSC23766 treated cells (6 extrusions each in phase 1 and 2). P values determined from log-rank test. See also Figures S2 and S3A-D.

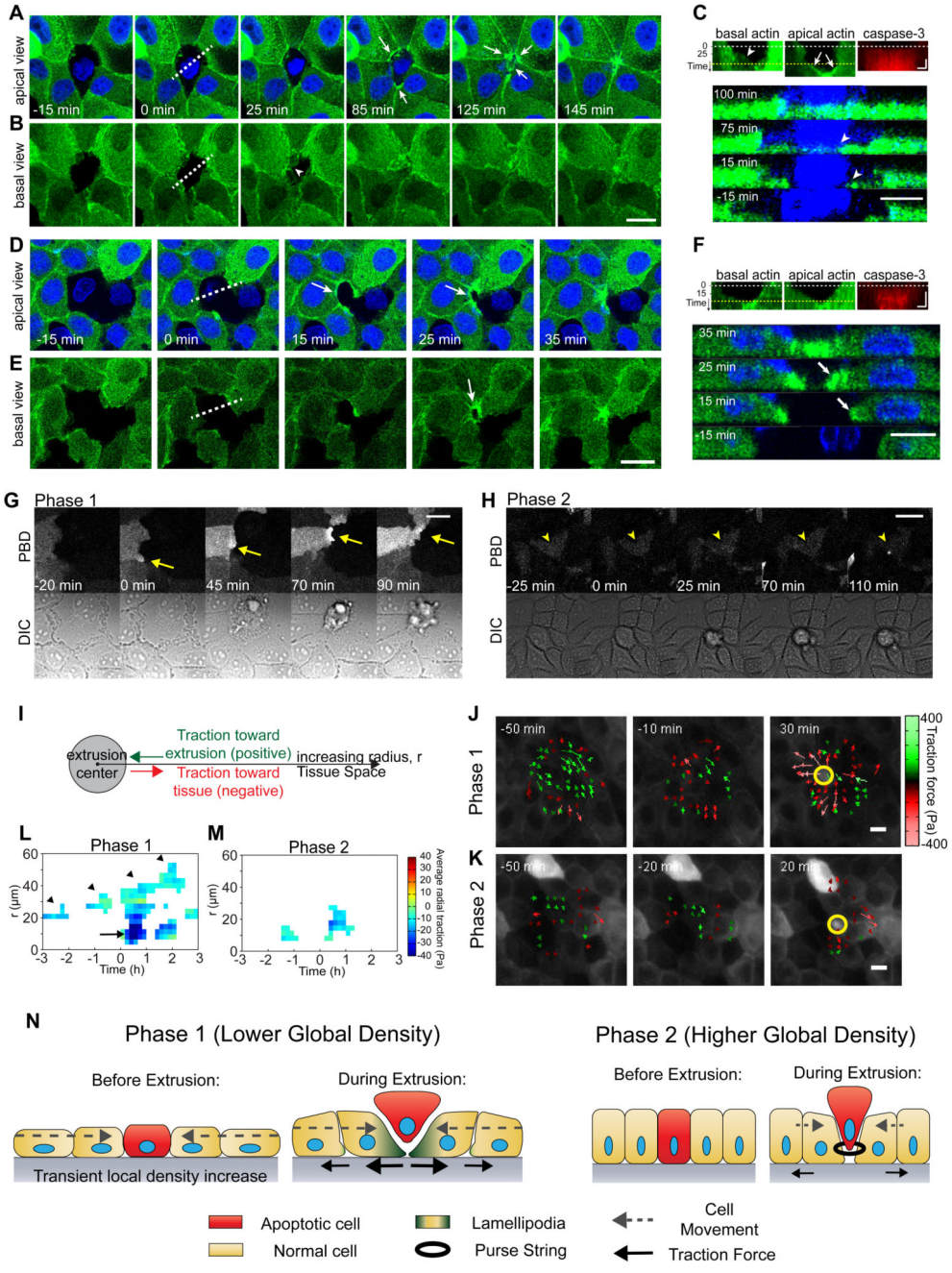

Figure 4. Lamellipodia-based crawling or purse-string mechanism depending on cell packing density

(A, B) Confocal images of an apoptotic extrusion during phase 1 with laser induction. Confluent layer of MDCK cells consist of WT (no GFP) and actin-GFP cells with nuclear staining (blue). t= 0 min indicates caspase-3 activation. Apical view (A) and basal view (B) highlight purse-string (arrows) and lamellipodia protrusion (arrowheads), respectively. (C-top panel) Kymograph of the basal and apical view of actin and caspase-3 generated from the dotted line in panels A and B. Note the lamellipodia protrusion (arrowhead) extended upon caspase-3 activation (t= 0 min) in the basal kymograph, and discontinuous actin cables

Europe PMC Funders Author Manuscripts

occurred (left, right arrows show two different timings) late in the extrusion. Yellow dotted line indicates basal region closed before apical region. (C-bottom panel) Side view of the extrusion process, arrowheads point to lamellipodia protrusion. (D-F) Corresponding confocal images of an apoptotic extrusion during phase 2. Apical view (D) and basal view (E) highlight purse-string (arrows). (F-top panel) Kymograph of the basal and apical view of actin and caspase-3 generated from the white dotted line in panels D and E. Yellow dotted line indicates basal region closed simultaneously with apical region closure. (F-bottom panel) Side view of the extrusion process, arrows point to actin accumulation and purse-string formation. Scale bars in panels B and E= 20 μm. Vertical and horizontal scale bars in C and F top panels denote 30 min and 5 μm, respectively. Scale bars in C and F bottom panels denote 10 μm. (G, H) Confocal images of a natural apoptotic extrusion in a confluent monolayer during phase 1 and 2, with PBD-YFP (top) and DIC (bottom) images. t= 0 min is time of extrusion, and arrows highlight the activation of PBD-YFP at the interface between neighbor and extruding cell in phase 1, while arrowheads point to location of extrusion, without clear PBD-YFP activation in the immediate neighbors. Scale bar = 20 μm (J) Schematic illustrating sign convention of traction force with respect to the center of extrusion. (J, K) Time evolution of actin fluorescence images of cell extrusion for phase 1 and 2, with traction field vectors overlaid. Extrusion (yellow circle) occurs at t= 0 hr, in the center of the image. Length of vector is proportional to traction magnitude, color code shows value of radial component with respect to extrusion as the center of radius. Scale bar = 10 μm. (L, M) Kymograph of average radial traction around extrusion (r= 0 μm, t= 0 hr), and averaged over all extrusion events. The same sign convention was used as in (J, K). The colored regions are regions with values significantly different when compared with the corresponding control (no extrusion) kymographs in Figure S3H, Supplemental Experimental Procedures. 5 different samples, 20 events for phase 1 and 39 events for phase 2. (N) Schematic representation describing the large-scale coordinated movements through cell crawling to extrude apoptotic cells at low density and switching to a local actomyosin contractile process of the immediate neighbors to drive extrusion at high density. The length of black arrows denotes the relative magnitude of traction forces, with smaller traction forces in phase 2. See also Figures S3E-H.

Europe PMC Funders Author Manuscripts